COMMUNICATIONS IN SCIENCE AND TECHNOLOGY
Homepage: cst.kipmi.or.id

Rotating speed and magnetic pole dependency assisted on copper deposition onto aluminum alloy substrate for bacterial eradication application

Basori[a,*], Ruliyanta[b], Maman Kartaman Ajiriyanto[c], Rosika Kriswarini[c], Heri Hardiyanti[c], Cahaya Rosyidan[d], Sigit Dwi Yudanto[e], Evi Ulina Margareta Situmorang[f], Daniel Edbert[g], Dwi Nanto[h], Ferry Budhi Susetyo[i]

[a]*Department of Mechanical Engineering, Universitas Nasional, Jakarta 12520, Indonesia*
[b]*Department of Electrical Engineering, Universitas Nasional, Jakarta 12520, Indonesia*
[c]*Research Center for Nuclear Material and Radioactive Waste Technology, National Research and Innovation Agency, Banten 15314, Indonesia*
[d]*Department of Petroleum Engineering, Universitas Trisakti, Jakarta 11440, Indonesia*
[e]*Research Center for Metallurgy, National Research and Innovation Agency, Banten 15314, Indonesia*
[f]*Department of Physiology School of Medicine and Health Sciences, Atma Jaya Catholic University of Indonesia, Jakarta 14440, Indonesia*
[g]*Department of Microbiology, Atma Jaya Catholic University of Indonesia, Jakarta 14440, Indonesia*
[h]*Department of Physics Education, UIN Syarif Hidayatullah, Jakarta 15412, Indonesia*
[i]*Department of Mechanical Engineering, Universitas Negeri Jakarta, Jakarta 13220, Indonesia*

Article history:
Received: 26 September 2024 / Received in revised form: 27 January 2025 / Accepted: 21 February 2025

Abstract

Copper (Cu) is widely used in many sectors, such as drinking water piping, heat exchangers, and medical equipment. The present research conducted an electrodeposition of Cu over an aluminum (Al) alloy substrate under the influence of various magnetic poles and rotating speeds. In the present study, a number of investigations, including deposition rate, current efficiency, coating thickness, surface morphology and phase, crystallographic orientation, antibacterial activity, electrochemical behavior, and hardness test were conducted. Increasing the rotation speed promoted to enhanced deposition rate and current efficiency for both magnetic poles influence. An increase in the deposition rate from 12.83 to 13.67 µm/h led to the increasing thickness, a change in surface morphology near the spheroidal, becoming a faceted structure. Presenting and rising in the rotation of a magnetic field led to a reduced surface roughness and crystallite size of Cu film for both magnetic poles influence. The Cu film made without spinning magnetic had a characteristic of highest bacterial inhibition zone around 2.50 ±0.56 cm². The CuRN50 sample had the lowest corrosion rate at around 0.055 mmpy, while the CuRS100 sample had the highest hardness value at approximately 80.72 HV for having the lowest crystallite size. Cu coated onto Al alloy could enhance its properties, such as being antimicrobial, being resistant against corrosion and having the hardness value.

Keywords: North and South Pole; SEM-EDS; XRD; electrochemical behavior; hardness

1. Introduction

Copper (Cu) due to its promising properties is widely used in many sectors, such as drinking water piping, heat exchangers, and medical equipment [1–3]. As film, it has a higher performance to kill bacteria compared to bulk Cu [4]. Additionally, coated onto aluminum (Al) alloy, Cu could enhance its properties, such as being antimicrobial, being resistant against corrosion and having hardness value [4,5]. Coating synthesis can be conducted by means of electrochemical, spin coating, or spray methods [6–8]. In view of its simplicity and affordability, the electrodeposition is seen as a more suitable method for coating Cu onto Al alloy [9].

Cu electrodepositions attract many researchers to investigate the formed Cu films. Brands *et al.* investigated the structure, surface morphology, electrical, optical, and magnetic properties of electrodeposited Cu_2O [10]. Antenucci *et al.* improved (the mechanical and thermal properties) of open-cell Al foams through Cu electrodeposition [11]. Augustin *et al.* investigated the effect of current density at Cu electrodeposition on the microstructure, hardness, and antibacterial activity of Cu for antimicrobial Al touch application [4]. Furthermore, Kuisor *et al.* fabricated CuO film using electrodeposition in which the film was tested for

* Corresponding author.
Email: basori@civitas.unas.ac.id
https://doi.org/10.21924/cst.10.1.2025.1547

antibacterial activity using *Staphylococcus aureus* (*S. aureus*) that successfully reduced the bacterial colony during the experiment [12]. Isa *et al.* performed electrodeposition Cu over 304 stainless steels in which a coated sample was tested for antibacterial properties. In a 10-minute exposure to the coated sample, it could successfully achieve a 100 % reduction of *S. aureus* [13].

Many factors, including magnetic field, determine the formed Cu films when electrodeposition is performed. The existing magnetic field at the electrodeposition process can appear to have several forces. The Lorentz force acts on a moving ion in the solution, resulting in convection flow [14]. The effects of the magnetic field may also relate to the electrokinetic-magnetohydrodynamic (MHD) effect resulting in the body force acting in the diffuse layer [15]. Another force caused by the magnetic field is paramagnetic gradient force [16] that causes the movement of magnetic ions in the diffusion layer. Another possible force is a magnetic gradient force. It acts on paramagnetic and diamagnetic ions [17]. In general, introducing a magnetic field during the electrodeposition process leads to the arrangement of moving ions towards the cathode.

In view of many forces exhibited by presenting a magnet, the investigations of several researchers have been focused on unrotated magnetic field-induced Cu electrodeposition [14,18–22]. Investigating the electrodeposition of Cu under 15 T of magnetic field, Miura *et al.* found extraordinary dendritic growth [19]. Murdoch *et al.* conducted an electrodeposition of Cu using the influence of 0.25 and 0.5 T placed on the working electrode's reverse, and this resulted in the lowest thickness when influencing 0.25 and 0.5 T with the south pole rather than the north pole [14]. Sudibyo *et al.* conducted the electrodeposition of Cu using the influence of 300 and 900 G (neodymium magnet), resulting in higher grain when electrodeposition Cu using the influence of 900 G [22]. Yin *et al.* investigated anomalous Cu hydride phase during the magnetic field-assisted electrodeposition of Cu. Presenting an anti-parallel magnetic field affecting the magnetohydrodynamic effect could enhance the hydrogen evolution and result in poor film quality [18]. Kovalyov *et al.* found that a weak magnetic field (0.5 and 0.7 mT) could affect the electrodeposition process, surface morphology, and texture [20]. Liu *et al.* stated that magnetic field-assisted electrodeposition could change hydrogen bond structure, reduce the charge transfer resistance, and increase the electrolyte viscosity [21].

Due to its ability to enhance the properties of films, electrodeposition assisted with a spinning magnetic field is considered to attract several researchers. Wang and Chen used 0.18 T of a magnetic field with various rotating speeds (1000-3000 rpm) when electrodeposition of nickel (Ni) and results presenting a magnetic field with various rotating speeds could decrease surface roughness [23]. Ji *et al.* fabricated Ni-SiC using an electrodeposition process and found that the exhibited rotating magnetic field made SiC particle distribution more uniform [24]. Syamsuir *et al.* stated that presenting a rotating magnetic field (500 and 800 rpm) at electrodeposition process could make surface morphology of the film more uniform [25]. They found that increasing the rotating speed of a magnetic field (one piece of neodymium magnet arranged spread five parts in the upside Teflon) at electrodeposition process could transform surface morphology from spheroidal to faceted structure [5].

Oxygen content on the Cu film surface can disrupt the transformation of Cu to Cu ions, reducing antibacterial performance [26]. The formation of surface morphology can have an impact on the antibacterial performance. Surface morphology, such as spheroidal and faceted structures, also contributes to the inhibition zone. A Cu film with spheroidal coating tends to create a higher inhibition zone [5].

The use of a magnetic field during electrodeposition can determine the movement of ions towards the cathode surface. Adjusting magnetic field rotation during electrodeposition also determines the ion movement. Furthermore, the different poles of the selected magnet also influence ion movement at electrodeposition process. Generally, the speed of ion movement can affect the properties of formed film. Based upon the literature review above, higher rotation was used (≥ 500 rpm) to influence the electrodeposition; for this, the present study used the speed rotation of 50 and 100 rpm. The speed rotation was chosen on the basis of previous study conducting Cu electrodeposition by means of barreling apparatus [27]. Syamsuir *et al.* used one piece of neodymium magnet arranged to spread five parts in the upside Teflon [5]. Therefore, the present research used more neodymium magnets to result in more influence of the magnetic field. Here, the influence of spinning using different magnetic poles was also not considered. Murdoch *et al.* found that different magnetic poles influenced the deposition process, resulting in different surface morphologies in Cu films [14]. Therefore, the present research comprehensively investigated the influence of the rotating speed and magnetic pole during Cu electrodeposition on the formation of the film for bacterial eradication applications. The electrodeposition of Cu was determined by various magnetic poles (north and south) and magnetic rotating speeds (0, 50, and 100 rpm). Several investigations were conducted using digital scales, scanning electron microscopy equipped with energy dispersive spectroscopy (SEM-EDS), X-ray diffraction, digital camera, optical microscope, potentiostat dan Vickers hardness.

2. Materials and Methods

2.1. Materials

Al alloy (0.106 wt.% Si, 0.365 wt.% Fe, 0.055 wt.% Cu, 0.043 wt.% Mn, 0.030 wt.% Mg, 0.003 wt.% Zn, 0.002 wt.% Ni, 0.018 wt.% Ti, 0.003 wt.% Pb, and Al balance) was used as cathode, while pure Cu was used as anode. Electrolyte solution was prepared by dissolving $CuSO_4.5H_2O$ (Merck) in deionized water. Electrolyte solution (250 ml of volume) was used for electrodeposition with the composition of 0.5 M $CuSO_4.5H_2O$ plus 20 ml of H_2SO_4.

2.2. Sample preparation

It began by cutting Al alloy into 2 × 2 cm for electrodeposition substrate using a shearing machine. Cu film was then made using a DC power supply (MDB PS-305DM) with 40 mA, and at 25°C, and pH 5.5 for one h. Cu films were

prepared under the influence of a clockwise rotating magnetic field, as seen in Fig. 1. The plating bath was placed on top of the rotation magnetic field equipment. Two pieces of neodymium magnet were stacked and arranged (six parts) in the upside Teflon, as seen in Fig. 1. One piece of neodymium magnet had 0.08 T of intensity (measured using gauss meter TD-8620). Five variation samples were made; one sample was made without the influence of a rotating magnetic field as a baseline. The sample was made by influencing 50 rpm and 100 rpm. Different pole variations were also used. Table 1 depicts the complete sample names.

Table 1. Sample name and remark

Sample name	Remark
CuR0	without the influence of a rotating magnetic field
CuRN50	50 rpm, north pole near the substrate
CuRN100	100 rpm, north pole near the substrate
CuRS50	50 rpm, south pole near the substrate
CuRS100	100 rpm, south pole near the substrate

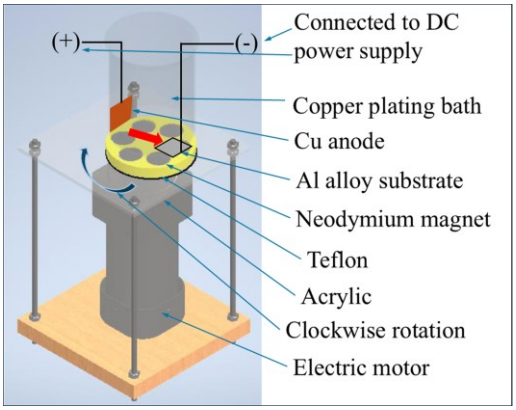

Fig. 1. Rotation magnetic field equipment

2.3. Characterizations

The deposition rate and current efficiency were measured similar to previous studies [17]. Thermo Scientific SEM-EDS was used to investigate surface morphology and elements. The cross section was also investigated using SEM apparatus to measure Cu layer thickness. According to SEM image, Image J software was used to measure grain distribution and the roughness of Cu film. Meanwhile, X-ray diffraction was conducted using PANalytical (Cu K radiation) with step size 0.02° and refined with the help of GSAS software [28].

Similarly, antibacterial activity was investigated according to previous studies [5]. The assessment of microbial reduction of various samples was adapted from ISO 22196 for non-porous material. *S. aureus* ATCC 25923 was used in this test. The inhibition zone was documented using a digital camera and assessed using an unaided eye and the area of inhibition was measured by Image J software. Each measurement was performed five times to ensure the data homogeneity. The diffusible area was calculated by subtracting the area of inhibition from the metal size. One-way ANOVA analysis was conducted to investigate whether there was significance between the polarities of the magnets. Moreover, the specimen was removed from the plate using sterile forceps. The agar was re-incubated at 35°C ±2 for 24 hours to observe the antimicrobial activity post-contact. The oxides of the metal formed before and after the test were observed by means of Olympus CX23 microscope under an 180 × magnification; any changes inside of the agar plate were documented. In addition, the observations of microbial reduction test were conducted (within 1, 2, 4, 6 and 12 h).

The electrochemical test was conducted using Ossila potentiostat in 0.9 % NaCl (room temperature). Prior to the electrochemical test, Cu films were mounted and left open area for 1 ×1 cm^2. Here, Cu films were used as working electrode, Ag/AgCl and Pt wire were used as reference electrode and counter electrode, respectively. There are two kinds of test in electrochemical behavior measurement, those are open circuit potential (OCP) and potentiodynamic polarization. OCP is performed until 1200 seconds, while potentiodynamic polarization is performed from -1 to -0.1 V using 5 mV/s of scan rate. The potentiodynamic polarization data was analyzed through the Tafel extrapolation method to find Icorr and Ecorr. Afterward, corrosion rate could be calculated using following equation [29].

$$\text{Corrosion rate (mmpy)} = K((a\ Icorr)/(n\ D)) \quad (1)$$

where K is constant (0.00327 mmpy), a is atomic weight, Icorr is corrosion current density (μA/cm^2), n is the number electron involved, and D is Cu density (g/cm^3).

The hardness test was performed using Future-Tech (FV-300e) Vickers hardness tester. Five repeatable measurements were conducted over Cu layer by using 1 kg of load.

3. Results and Discussion

3.1. Deposition rate and current efficiency

Fig. 2 shows the deposition rate and current efficiency of electrodeposition Cu over an Al alloy substrate. They had similar tendencies; an increase in magnet rotation speed led to a rise in deposition rate and current efficiency.

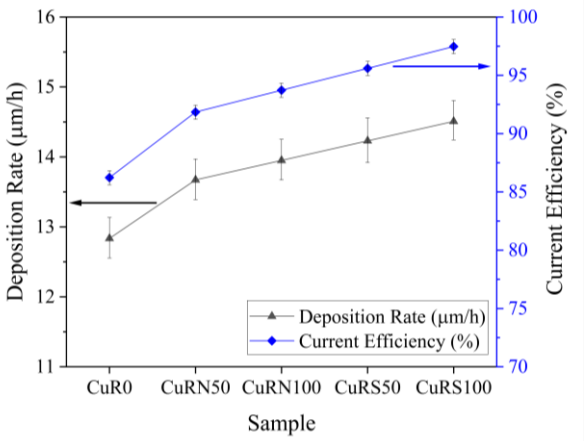

Fig. 2. Deposition rate and current efficiency of Cu electrodeposition

In the process of Cu electrodeposition, the oxidation process occurs at the anode and a reduction process occurs at the cathode. An Al alloy (substrates) to be plated is placed at

the cathode. When the current is applied, the Cu ions are depleted in the surroundings of the cathode, making a diffusion film upper around the cathode. Hydrogen evolution is known to occur at the cathode during Cu electrodeposition from aqueous solutions [17]. Less hydrogen evolution can increase the deposition rate and current efficiency because hydrogen evolution is able to disturb the movement of the ions to the cathode [30,31]. Presenting an anti-parallel magnetic field (north pole) affecting the MHD effect could enhance the hydrogen evolution, decrease current efficiency, and result in poor film quality [18]. As shown in Fig. 2, hydrogen evolution seemed to influence the electrodeposition process when being determined by the north pole. Therefore, the electrodeposition process had a lesser current efficiency than the electrodeposition process when being influenced by the south pole.

Cu films made and influenced by the rotating south pole magnet has a higher deposition rate due to the magnetic field, which was parallel to the current direction and attracts more Cu ions onto the Al alloy surface [14]. Rotating the magnet under the electrolyte solution during the electrodeposition process could induce an Eddy electric field [5] that can act as an additional MHD flow convection effect [23]. Moreover, increasing the rotation speed could attract more Cu ions onto the Al alloy surface, consequently increasing the deposition rate and current efficiency.

3.2. Average thickness

Fig. 3 and Fig. 4 show the thickness of various Cu layers and average thickness of Cu layers. Compared to the average thickness to the deposition rate (Fig. 2), there was a correlation between them. Increasing the deposition rate led to an increase in the average of Cu layers thickness, similar to the study by Syamsuir *et al.* [27]. Furthermore, it seemed that average coating thickness was higher than thickness found by calculating from deposition rate. For example, average coating thickness of CuR0 sample ideally is 12.83 µm due to deposition sample for one hour. Unfortunately, average coating thickness of CuR0 sample was 27.17 µm. This behavior was probably due to the SEM cross section being conducted on an area near the anode (red arrow Fig. 1). According to Yang *et al.*, the end area of the cathode results in higher thickness compared to the middle area [32]. Therefore, average thickness is higher than deposition rate value.

3.3. SEM-EDS and roughness

Fig. 5 shows the SEM result and the grain distribution of various Cu film surfaces. Samples were made by influencing the north pole magnetic field, which had a larger grain size than samples created by affecting the south pole of a magnetic field. Generally, presenting the south pole magnetic field influence can lead to a decrease in grain size. While presenting south pole magnetic field influence can lead to an increase in grain size as in line with previous study [33]. Murdoch *et al.* stated that different poles are used to influence deposition process that will result different grain size [14]. Moreover, Lin *et al.* stated that deposition time contributes to the formed grain size [34].

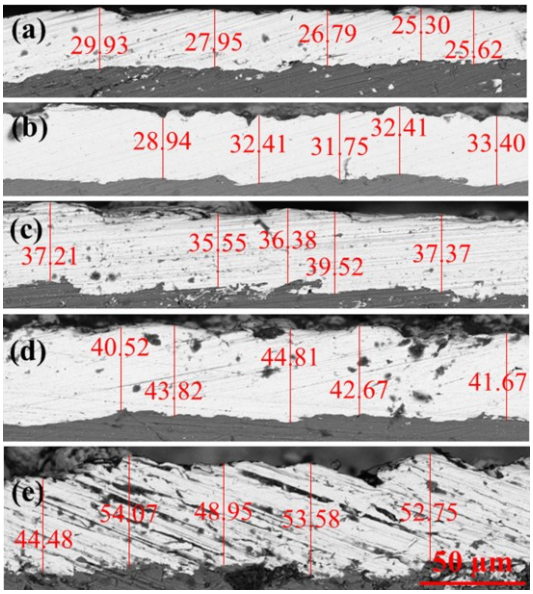

Fig. 3. Thickness of various Cu layers: (a) CuR0; (b) CuRN50; (c) CuRN100; (d) CuRS50; and (e) CuRS100

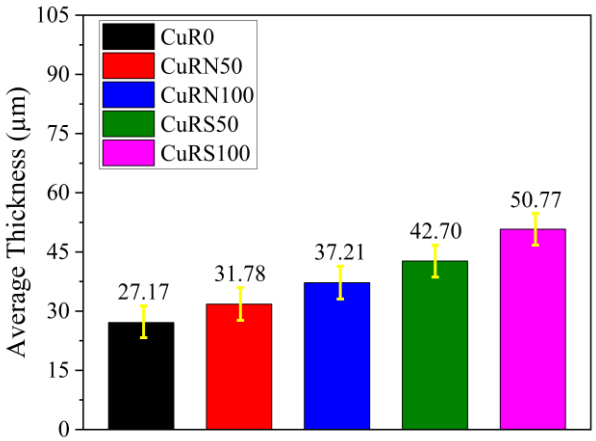

Fig. 4. Cu layers average thickness

As shown in Fig. 5, the Cu sample was made with no spinning magnetic influence, leading to the formation of morphology near the spheroidal. Cu samples made with spinning magnetic assistance led to the formation of faceted structure morphology [17]. Moreover, the transformation from spheroidal to faceted structure was determined by the deposition rate. A higher nucleation rate leads to a higher deposition rate, resulting in a variation in surface morphology [35]. Samples made with influences from the north pole magnetic field had a low nucleation rate. Hence, it had wider grain sizes than samples by influencing the south pole magnetic field [14]. Moreover, an increase in the deposition rate from 12.83 to 13.67 µm/h led to a change in surface morphology near the spheroidal becoming faceted structure. The deposition rate between 13.67 and 14.51 µm/h resulted in a faceted structure of surface morphology.

The south pole had an affecting magnetic field parallel to the current direction; therefore, Cu ions were more attracted to the Al alloy surface. In contrast, the north pole had an affecting magnetic field that was anti-parallel to the current direction, reducing Cu ions' attraction onto the Al alloy

surface. Moreover, Lorentz's forces rotated opposite each other on top of the surface specimen for different magnetic poles. This condition affected the sample film by influencing the South Pole to be smoother than the North Pole. Ji *et al.* stated that presenting a rotating magnetic field during electrodeposition can make surface morphology more uniform [24]. In this case, the paramagnetic force has a similar tendency for different magnetic poles. Therefore, influencing surface morphology could be neglected.

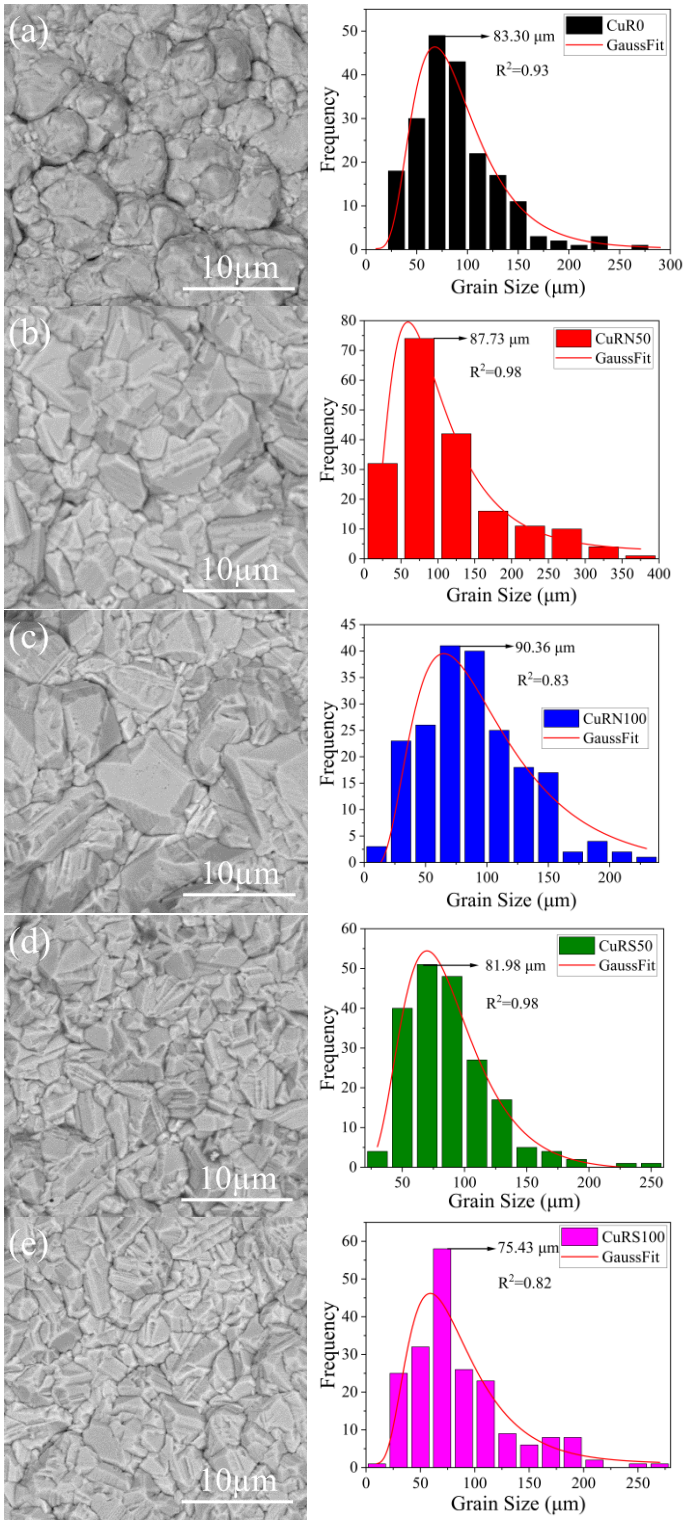

Fig. 5. SEM and grain distribution of Cu layers: (a) CuR0; (b) CuRN50; (c) CuRN100; (d) CuRS50; and (e) CuRS100

As shown in Fig. 6, the spinning magnetic-assisted running at 50 rpm led to oxygen formed on the Cu surface. Moreover, enhanced magnetic rotation led to a decrease or disappearance of oxygen. Presenting oxygen on Cu film is one of the unique cases in which oxygen can be formed due to both a secondary reaction on the anode and sample storage and transport [5].

Fig. 7 presents the roughness analyzed result from the SEM image using ImageJ software. CuR0, CuRN50, CuRN100, CuRS50, and CuRS100 samples had a surface roughness of 34.62, 18.00, 17.38, 18.60, and 16.58 μm, respectively. Presenting a magnetic field rotation during electrodeposition led to a decrease in the surface roughness of Cu film. More rotation could also decrease surface roughness, which is perfectly in line with the previous study [5]. Wang and Chen found that presenting a magnetic field during electrodeposition with various rotating speeds could decrease surface roughness [23]. This behavior is probably due to additional MHD flow, which is in line with the deposition rate result and could enhance the Cu ions' movement. A higher deposition rate would result in a higher nucleation rate, consequently producing a smooth surface morphology. Moreover, the sample made by north pole magnet influence had more roughness than sample made by north pole magnet. This behavior probably due to MHD effect that could enhance the hydrogen evolution and result in more roughness [18].

3.4. X-ray diffraction

Fig. 8 shows the diffraction patterns of samples of Cu deposition on substrates consisting of Al alloy plates. The five samples were identified to have Cu phase peaks at the indexed plane peaks (111), (200), (220), (311), and (222) at angles 2θ = 43.31, 50.45, 74.13, 89.94, and 95.15°. The cubic crystal system was found in the Cu phase, and it had a space group of fm-3m. The cubic Cu phase peaks at these angles were found consistent with the findings from studies by Omar and Francisco Briones *et al.* [36,37]. This demonstrated that the procedure for depositing Cu on Al alloy plates has been successfully completed. At the indexed plane peaks (111), (200), (220), (311), and (400) of the five diffraction patterns, they were also found on the Al alloy plate substrate along with the copper phase. Xu *et al.* and Ayieko *et al.* presented a standard Al diffraction pattern identical to this peak of Al [38,39].

The mean crystallite size and lattice value of the five deposition samples were compared to further analyze the diffraction pattern. The Rietveld method was employed to determine the lattice of the five samples. The cubic Cu phase lattice of all five samples was measured at 0.3615 nm based upon the calculation results. Changes in magnetic poles and rotating speed showed no effect on the lattice value of the cubic Cu phase. Table 2 presents the data from the crystallographic calculation. To determine the mean crystallite size, the Williamson-Hall plot method was utilized. In contrast to the lattice value, the mean crystallite size was affected by the rotating speed and poles. The mean crystallite size became finer with the increase in magnet rotation speed perfectly matched with surface roughness analysis.

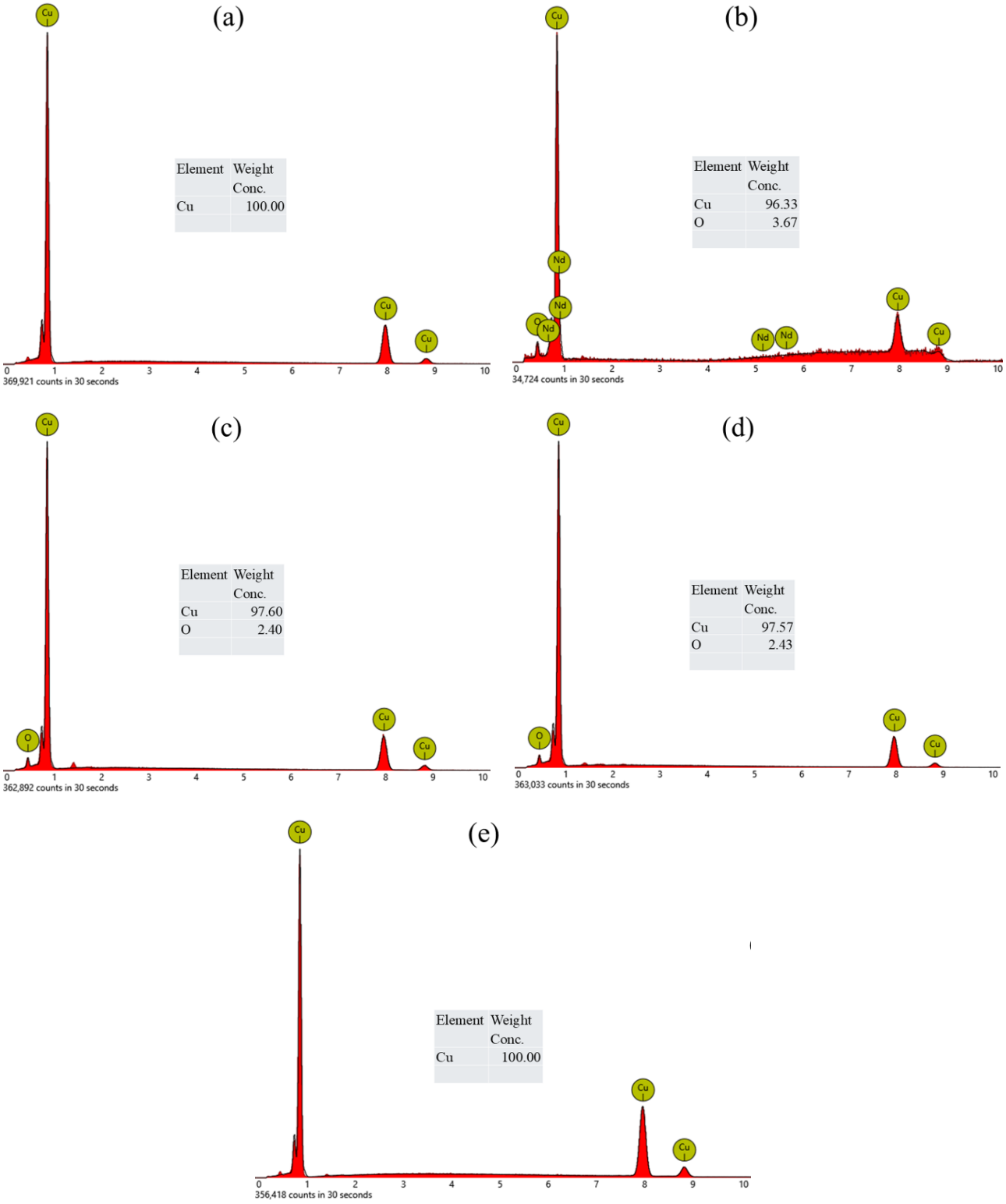

Fig. 6. EDS Cu layers: (a) CuR0; (b) CuRN50; (c) CuRN100; (d) CuRS50; and (e) CuRS100

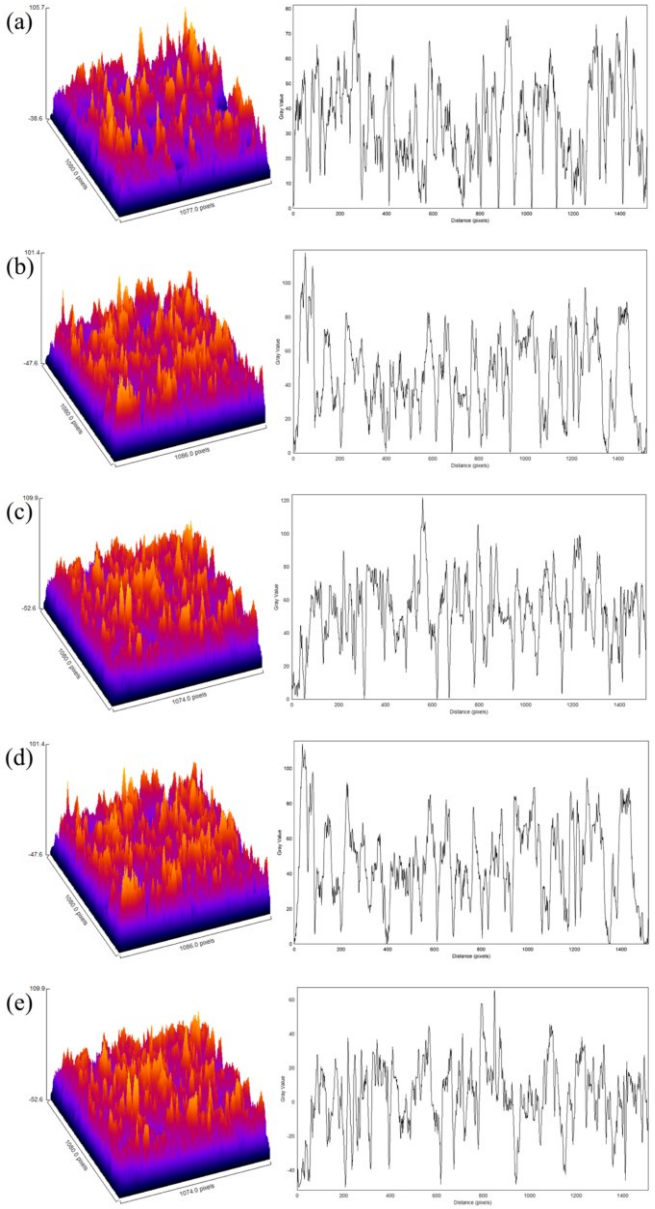

Fig. 7. Roughness Cu layers: (a) CuR0; (b) CuRN50; (c) CuRN100; (d) CuRS50; and (e) CuRS100

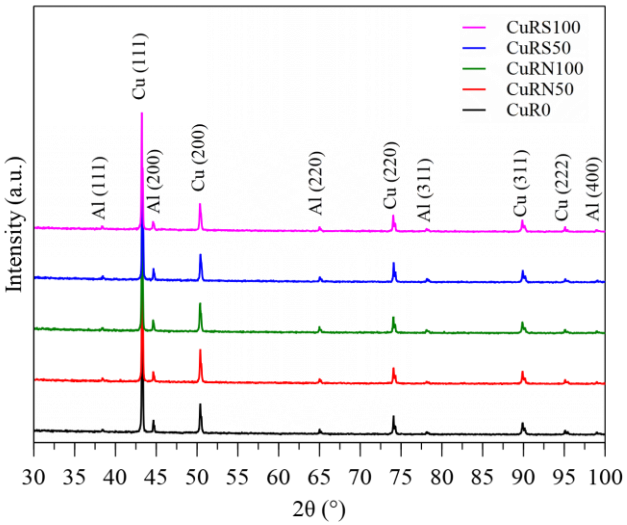

Fig. 8. X-ray diffraction pattern of various sample

Table 2. Crystallographic data calculated from various samples

Source	CuR0	CuRN50	CuRN100	CuRS50	CuRS100
Phase	Name: Copper (Cu) Space group: F m -3 m (225) Crystal system: cubic				
Lattice -a (nm)	0.3615	0.3615	0.3615	0.3615	0.3615
wRp (%)	10. 10	10.37	10.24	9.86	10.30
GoF	1. 067	1.106	1.087	1. 045	1.056
Mean crystallite size (nm)	308	173	154	173	126
Micro-strain (%)	0.07	0.05	0.05	0.05	0.04

3.5. Antibacterial activity

Fig. 9 describes the antibacterial activity test after 24 hours of contact. Material placement in the middle of Mueller Hinton agar was inoculated with *S. aureus* ATCC 25923. Noticing the inhibition zones around the material; the calculation is presented in Table 3. The metal ions were diffused into the agar to inhibit the growth of *S. aureus*.

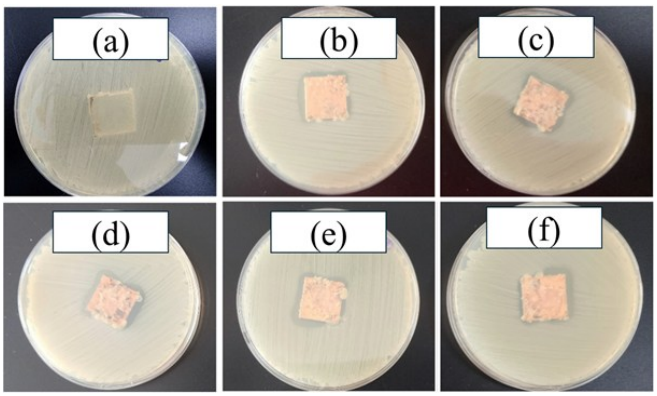

Fig. 9. Antibacterial activity test after 24 hours: (a) blank; (b) CuRN50; (c) CuRN100; (d) CuR0; (e) CuRS50; and (f) CuRS100

Cu, particularly in the form of metal-organic frameworks (MOFs) and nanoparticles, exhibited significant antibacterial activity against Gram-positive bacteria such as *S. aureus* [40]. The peptidoglycan layer in Gram-positive bacteria plays a significant role in their susceptibility to Cu although its direct interaction with Cu is not as straightforward as with other antimicrobial agents. Cu is able to induce modifications in the peptidoglycan layer, such as increased cross-linkage, which can affect the overall structure and function of the cell wall. These modifications can either enhance or reduce the susceptibility of Gram-positive bacteria to Cu, dependent on the specific bacterial strain and environmental conditions [41,42]. In this research, the Cu induced contact killing. The antimicrobial activity of Cu is believed to involve contact-mediated killing, initiating membrane degradation. The susceptibility of Gram-positive strains to Cu is attributed to the thick peptidoglycan layer, reducing cell wall permeability to other metal ions, including Zinc [43].

As shown in Fig. 9, the inoculum was totally annihilated by electroplated materials. The log reduction was not calculated due to the total killing of the bacteria. However, the total reduction of > 105 CFU/ml might suggest a percentage reduction of > 99.999% (see Table 3). Moreover, there was a zone of inhibition between the sample and bacterial lawn that was also visible inside the zone's white crystals and some bluish color change inside the agar. This suggests that the Cu material diffused and interacted with the agar can result in a zone of bacterial growth inhibition.

As seen in Table 3, the widest diffusion zone was observed in CuR0 with the zone of diffusion and inhibition areas of 6.99 cm^2 and 2.5 cm^2. This was statistically significant with $p < 0.001$ (ANOVA; CI 95%). Also, there was significance in independent T-Test analyses between CuR0 and CuR50 group ($p < 0.001$; CI 95%), R0 and R100 group ($p < 0.001$; CI 95%), and between CuR50 and CuR100 Group ($p < 0.001$; CI 95%). To investigate whether there was significance between the polarities of the magnets, independent T-test analyses were performed. There was no significant difference in the outcome between the south pole group and the north one ($p=0.063$; CI 95%). Moreover, there were no inhibitions in the blank group, and the bacteria grew underneath the metal. Comparing to the previous study, less inhibition was found in the present study [5]. This behavior was probably due to higher crystallite size form in the all samples [44]. Previous study found crystallite size between 95.66 and 100.50 nm [5]. While in the present study, the crystallite size of Cu layer was between 126 and 308 nm. Ramyadevi *et al.* and Ahmed *et al.* in their studies, when testing Cu nanoparticle for antibacterial activity using *S. aureus*, found the inhibition zone of 2.2 cm and 2.4 cm [45,46].

Table 3. The reduction of colony, and diffusible metal observation

Sample	Microbial reduction assessment		Diffusible metal observation	
	Initial load 0 h (CFU/ml)	Final load 24 h (CFU/ml)	Zone of diffusion (cm^2)	Inhibition area (cm^2)
Blank	3.5×10^5	0	4.01 ±0.01	-0.48 ±0.01
CuR0		0	6.99 ±0.12	2.50 ±0.56
CuRN50		0	6.21 ±0.01	1.61 ±0.21
CuRN100		0	6.00 ±0.02	1.89 ±0.02
CuRS50		0	6.16 ±0.41	1.73 ±0.46
CuRS100		0	6.17 ±0.01	2.14 ±0.24

The use of magnetic rotation during material synthesis showed a significant impact on the results. Materials synthesized without magnetic rotation (R0) showed the stronger antibacterial effects compared to those synthesized at 50 rpm or 100 rpm. However, increasing magnet rotation significantly enhanced the size of the inhibition zone. As a result, the inhibition zone at 100 rpm was found larger than that of at 50 rpm. This condition was probably due to forming some oxygen on the Cu films surface as seen in EDS result, which could disrupt transformation Cu to be Cu ions. Qu *et al.* found that antibacterial behavior was determined by Cu ions [26]. The release of Cu ions inside of the agar was lethal towards *S. aureus* [47].

As shown in Fig. 3, CuR0 surface morphology formed near to spheroidal, while other samples formed a faceted structure. In Table 3, it can be seen that higher inhibition zone was seen in CuR0 sample. Therefore, it can be concluded that the spheroidal form results in the higher inhibition zone compared to faceted structure, which is perfectly in agreement with previous study [5]. This condition probably occurred due to the spheroidal structure having a wider surface area than the faceted structure, where more Cu ions were released. Moreover, an increase in rotation leads to a decrease in roughness. Several researchers have found that roughness is independent of the inhibition zone, which aligns with the present study [5,48].

Moreover, the generation of reactive oxygen species (ROS) and damage to cell membranes are the main ways in which metals' broad antibacterial potential has been extensively studied [49–51]. Even so, metals can target particular cellular components and, when combined, are likely to improve pathogen clearance despite their non-specific activity. Conversely, Cu has an ability to change metabolic pathways in addition to cause damage to DNA and cell membranes through the generation of ROS [52]. The combined mode of action has not been investigated so far, despite the fact that the modes of action of various metal ions have been well explored. The variability in antimicrobial efficaciousness between various combinations can be explained by the diverse chemical reactivity of metal ions with bacterial cells and their specific biological targets [53].

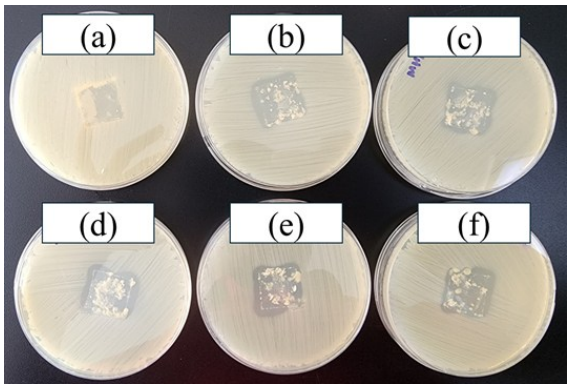

Fig. 10. After 24 hours of post contact test: (a) blank; (b) CuRN50; (c) CuRN100; (d) CuR0; (e) CuRS50; and (f) CuRS100

Fig. 10 shows the results after 24 hours of post-contact testing. The inhibitory zones appeared after the removal of the material. There were some metal infiltrations inside the agar on every plate making the agar cracked. This indicated gas-forming or exothermic reaction inside the agar, increasing the antimicrobial ability of the material [54]. There were no anti-Staphylococcal effects on the blank material; therefore, there was a regrowth of microorganisms in the place where the metal was previously placed.

Fig. 11 shows antibacterial activity pretest microscope observation, and Fig. 12 shows antibacterial activity post-test microscope observation. The microscopic observation of electroplated surfaces occurred under an 180 × magnification

optical microscope. There was a significant proportion in the formation of white crystals on the electroplated surface after tests. The crystals did not form on the surface of the blank. The Cu formed oxides, which changed the surface color. Marković et al. stated that color change in the Cu is in relation to adsorption or reduction Cu ions [55].

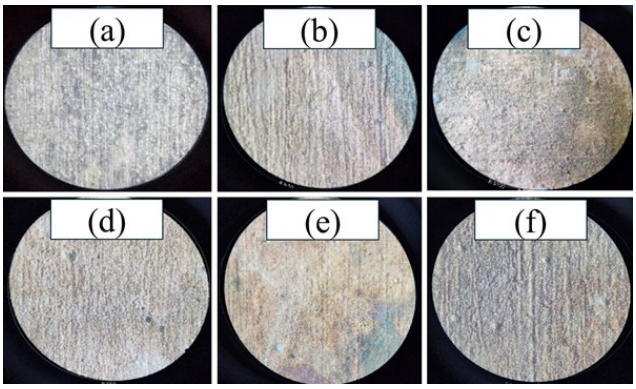

Fig. 11. Antibacterial activity pretest microscope observation: (a) blank; (b) CuRN50; (c) CuRN100; (d) CuR0; (e) CuRS50; and (f) CuRS100

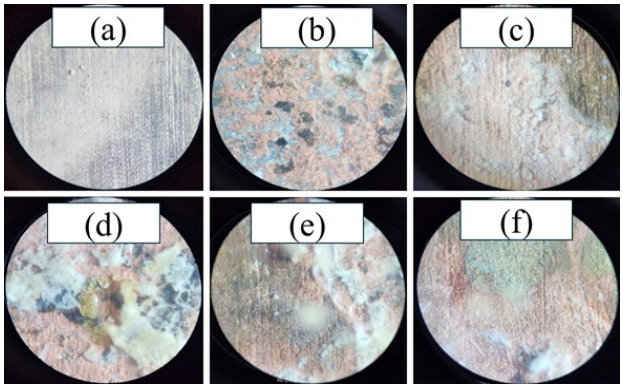

Fig. 12. Antibacterial activity post-test microscope observation: (a) blank; (b) CuRN50; (c) CuRN100; (d) CuR0; (e) CuRS50; and (f) CuRS100

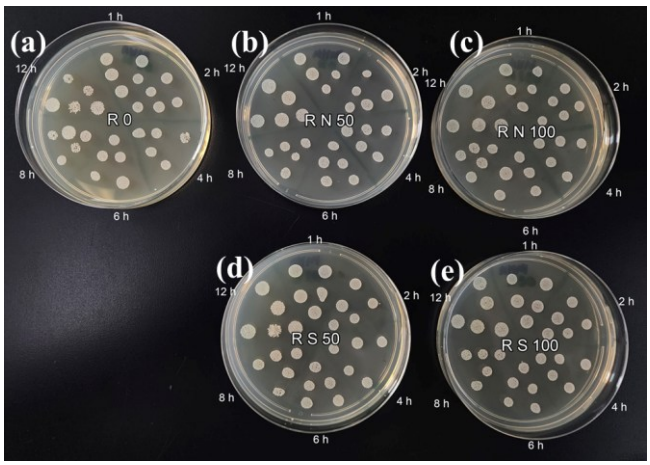

Fig. 13. Microbial reduction test observation: (a) CuR0; (b) CuRN50; (c) CuRN100; (d) CuRS50; and (e) CuRS100

As seen in Fig. 13 and Table 4, to deep explore microbial reduction assessment, investigating at 1, 4, 6, 8, and 12 hours were conducted. At 6 hours of investigation, CuR0 sample resulted in a reduction colony-forming units per milliliter around 10^4, which was in line with inhibition area value (higher inhibition area). While other samples still showed similar results when initial exposure occurred (See Table 3).

Table 4. Microbial reduction assessment of Cu samples

Sample name	1 h	2 h	4 h	6 h	12 h
			(CFU/ml)		
CuR0	$>10^5$	$>10^5$	$>10^5$	10^4	10^4
CuRN50	$>10^5$	$>10^5$	$>10^5$	$>10^5$	$>10^5$
CuRN100	$>10^5$	$>10^5$	$>10^5$	$>10^5$	$>10^5$
CuRS50	$>10^5$	$>10^5$	$>10^5$	$>10^5$	$>10^5$
CuRS100	$>10^5$	$>10^5$	$>10^5$	$>10^5$	$>10^5$

3.6. Electrochemical behavior

Fig. 14 shows the OCP measurement result of various Cu samples. E_{OCP} values of the CuR0, CuRN50, CuRN100, CuRS50, and CuRS100 were -0.643, -0.667, -0.658, -0.633, and -0.641 V vs Ag/AgCl, respectively. Previous study found E_{OCP} of Cu layer over Al alloy between -0.694 and -0.684 V vs Ag/AgCl [27]. All samples showed a shift to more negative value to reach a steady state. Tasić *et al.* stated that this condition implies the Cu oxide dissolution and CuCl layer formation [56]. The CuRN50 layer seemed more stable than other sample, showing to reach steady state at around 600 s for OCP measurement.

Fig. 15 represents potentiodynamic polarization test result in 0.9 % NaCl. Table 4 presents the tafel extrapolation result. Using Eq. (1), corrosion rate was calculated and summarized in Table 5.

As shown in Table 5, the CuRN50 sample was found as the sample with the lowest corrosion rate, probably due to the highest oxygen on the Cu surface that could form an oxide [57]. Narayanan *et al.* stated that oxygen content in the Cu film would be an obstacle for chloride ions to adsorb in the film [58]. Therefore, the oxide could result in better protection from aggressive species in the 0.9 % NaCl medium. Moreover, compared to Fig. 6, the oxygen content of the Cu layer was linear to the corrosion rate. Higher oxygen content led to decrease corrosion rate.

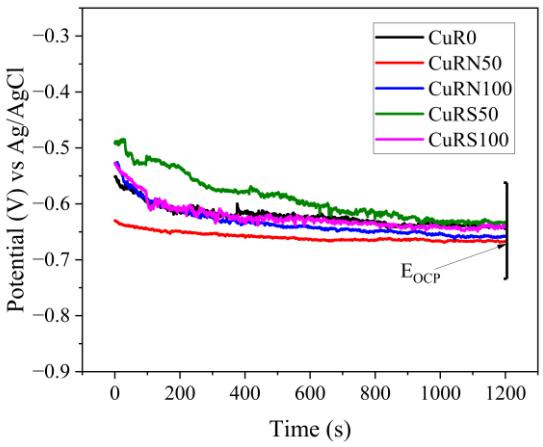

Fig. 14. OCP test curve

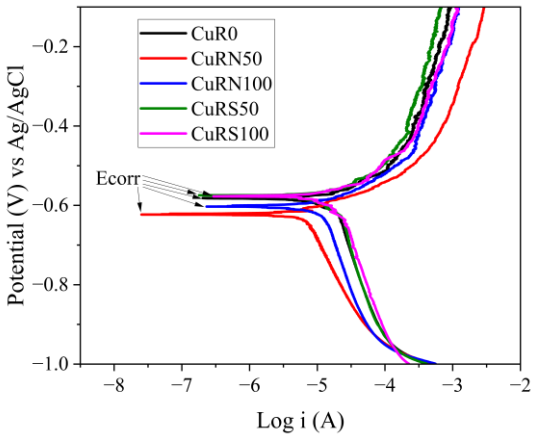

Fig. 15. Potentiodynamic polarization test curve

Table 5. Tafel extrapolation result and corrosion rate

Sample name	Ecorr (V) vs Ag/AgCl	Icorr (A/cm²)	Corrosion rate (mmpy)
CuR0	-0.582	1.27×10^{-5}	0.148
CuRN50	-0.623	4.78×10^{-6}	0.055
CuRN100	-0.603	8.77×10^{-6}	0.102
CuRS50	-0.574	8.56×10^{-6}	0.099
CuRS100	-0.577	1.14×10^{-5}	0.132

3.7. Hardness test

Fig. 16 represents average hardness test result using 1 kg of load. The hardness test was conducted with five repeatable measurements on top of Cu layer. The average hardness in the present study varied between 47.92 and 80.72 HV. Ghosh et al. found that Cu layer hardness from 22.9 to 114.7 HV [59]. Previous study also found Cu layer hardness between 72.94 and 76.26 HV [5]. Moreover, Augustine *et al.* stated that hardness value is dependent on the crystallite size. The lowest crystallite size promoted to resulting higher hardness [4]. Comparing Fig. 16 to Table 2, there was a linear correlation between hardness and crystallite size. Highest hardness value was seen at CuRS100 sample, while smallest one was found at CuR0 sample.

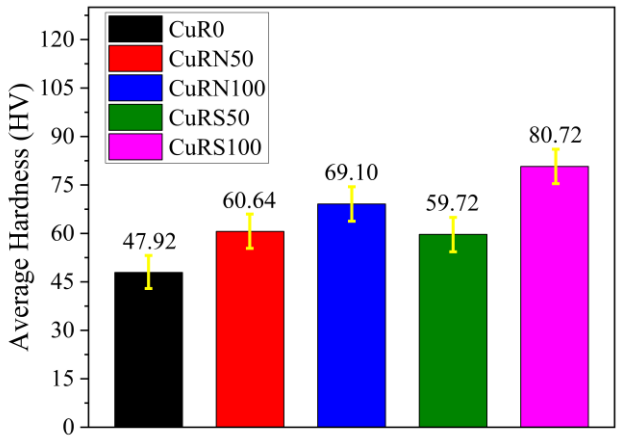

Fig. 16. Average of the hardness test result

4. Conclusion

This study has successfully conducted the Cu films fabricated under a spinning magnetic field with various rotation speeds and a magnetic pole. Higher rotation speed was promoted to enhance deposition rate and current efficiency for both magnetic poles. The Cu sample fabricated with no spinning magnetic influence led to the morphology formed near the spheroidal. Cu samples made with spinning magnetic influence led to the morphology formed near the faceted structure. Magnetic-assisted spinning at 50 rpm led to oxygen formed on the Cu surface for both magnetic poles and enhanced rotation. This then led to the decrease or disappearance of oxygen. Presenting and rising in magnetic field rotation led to decreased surface roughness and crystallite size of Cu film for both magnetic poles. The Cu sample made without spinning magnetic fields influence had the highest inhibition zone size, probably due to the absence of oxygen on the Cu film surface and the morphology near the spheroidal. The oxygen content of the Cu layer was found linear to the corrosion rate. Higher oxygen content led to decrease corrosion rate, while the lowest crystallite size promoted to higher hardness. Overall, Cu films successfully covered Al alloy and could transform it into antibacterial material. For future study, it is recommended to conduct the electrodeposition of Cu with spinning magnetic influence higher than 100 rpm.

Acknowledgements

This study has been supported by the Ministry of Education, Culture, Research, and Technology through grand funding Penelitian Fundamental-Regular with contract number 087/LPPM-UNAS/VI/2024 and 815/LL3/AL.04/2024.

References

1. D. A. Lytle and C. P. White, *The effect of phosphate on the properties of copper drinking water pipes experiencing localized corrosion*, J. Fail. Anal. Prev. 14 (2014) 203–219.
2. M. M. Lachowicz, *A metallographic case study of formicary corrosion in heat exchanger copper tubes*, Eng. Fail. Anal. 111 (2020) 104502.
3. N. Thokala, C. Kealey, J. Kennedy, D. B. Brady and J. B. Farrell, *Characterisation of polyamide 11/copper antimicrobial composites for medical device applications*, Mater. Sci. Eng. C 78 (2017) 1179–1186.
4. A. Augustin, P. Huilgol, K. R. Udupa and U. B. K, *Effect of current density during electrodeposition on microstructure and hardness of textured Cu coating in the application of antimicrobial Al touch surface*, J. Mech. Behav. Biomed. Mater. 63 (2016) 352–360.
5. Syamsuir, F. B. Susetyo, B. Soegijono, S. D. Yudanto, Basori, M. K. Ajiriyanto et al., *Rotating-Magnetic-Field-Assisted Electrodeposition of Copper for Ambulance Medical Equipment*, Automot. Exp. 6 (2023) 290–302.
6. A. M. Alghamdi and F. Fadhillah, *Thin film composite polyelectrolyte multilayer nanofiltration membrane fabricated using spin assisted layer by layer assembly: Application of solution diffusion film model*, Commun. Sci. Technol. 5 (2020) 10–15.

7. C. Santoso, Ratnawati and Slamet, *Utilization of glycerol solution for hydrogen production by a combination of photocatalysis and electrolysis processes with Fe-TiO2 nanotubes*, Commun. Sci. Technol. 8 (2023) 208–215.
8. W. Trisunaryanti, K. Wijaya and A. M. Tazkia, *Preparation of Ni/ZSM-5 and Mo/ZSM-5 catalysts for hydrotreating palm oil into biojet fuel*, Commun. Sci. Technol. 9 (2024) 161–169.
9. A. Lelevic and F. C. Walsh, *Electrodeposition of Ni-P alloy coatings: A review*, Surf. Coatings Technol. 369 (2019) 198–220.
10. I. S. Brandt, M. A. Tumelero, S. Pelegrini, G. Zangari and A. A. Pasa, *Electrodeposition of Cu2O: growth, properties, and applications*, J. Solid State Electrochem. 21 (2017) 1999–2020.
11. A. Antenucci, S. Guarino, V. Tagliaferri and N. Ucciardello, *Improvement of the mechanical and thermal characteristics of open cell aluminum foams by the electrodeposition of Cu*, Mater. Des. 59 (2014) 124–129.
12. A. Kusior, J. Mazurkow, P. Jelen, M. Bik, S. Raza, M. Wdowiak et al., *Copper Oxide Electrochemical Deposition to Create Antiviral and Antibacterial Nanocoatings*, Langmuir 40 (2024) 14838–14846.
13. N. N. C. Isa, Y. Mohd, M. H. M. Zaki and S. A. S. Mohamad, Antibacterial activity of copper coating electrodeposited on 304 stainless steel substrate, in AIP Conference Proceedings, 1901 (2017), pp. 020009.
14. H. A. Murdoch, D. Yin, E. Hernández-Rivera and A. K. Giri, *Effect of applied magnetic field on microstructure of electrodeposited copper*, Electrochem. commun. 97 (2018) 11–15.
15. Q. Long, Y. Zhong and J. Wu, *Research progress of magnetic field techniques for electrodeposition of coating*, Int. J. Electrochem. Sci. 15 (2020) 8026–8040.
16. K. Kołodziejczyk, E. Miękoś, M. Zieliński, M. Jaksender, D. Szczukocki, K. Czarny et al., *Influence of constant magnetic field on electrodeposition of metals, alloys, conductive polymers, and organic reactions*, J. Solid State Electrochem. 22 (2018) 1629–1674.
17. B. Soegijono, F. B. Susetyo, Yusmaniar and M. C. Fajrah, *Electrodeposition of paramagnetic copper film under magnetic field on paramagnetic aluminum alloy substrates*, e-Journal Surf. Sci. Nanotechnol. 18 (2020) 281–288.
18. D. Yin, H. A. Murdoch, B. Chad Hornbuckle, E. Hernández-Rivera and M. K. Dunstan, *Investigation of anomalous copper hydride phase during magnetic field-assisted electrodeposition of copper*, Electrochem. commun. 98 (2019) 96–100.
19. M. Miura, Y. Oshikiri, A. Sugiyama, R. Morimoto, I. Mogi, M. Miura et al., *Magneto-Dendrite Effect: Copper Electrodeposition under High Magnetic Field*, Sci. Rep. 7 (2017) 1–8.
20. S. V. Kovalyov, O. B. Girin, C. Debiemme-Chouvy and V. I. Mishchenko, *Copper electrodeposition under a weak magnetic field: effect on the texturing and properties of the deposits*, J. Appl. Electrochem. 51 (2021) 235–243.
21. Y. Liu, B. Zheng, T. Zhang, Y. Chen, J. Liu, Z. Wang et al., *Magnetic field intensified electrodeposition of low-concentration copper ions in aqueous solution*, Electrochim. Acta 432 (2022) 141201.
22. Sudibyo, M. B. How and N. Aziz, Influences of magnetic field on the fractal morphology in copper electrodeposition, in IOP Conference Series: Materials Science and Engineering, 285 (2018), pp. 012021.
23. T. Wang and W. Chen, *Effects of Rotating Magnetic Fields on Nickel Electro-Deposition*, ECS Electrochem. Lett. 4 (2015) D14–D17.
24. R. Ji, K. Han, H. Jin, X. Li, Y. Liu, S. Liu et al., *Preparation of Ni-SiC nano-composite coating by rotating magnetic field-assisted electrodeposition*, J. Manuf. Process. 57 (2020) 787–797.
25. S. Syamsuir, F. B. Susetyo, B. Soegijono, S. D. Yudanto, Basori and D. Nanto, Nickel layers properties produced by electroplating were influenced by spinning permanent magnet, in Journal of Physics: Conference Series, 2596 (2023), pp. 012008.
26. X. Qu, H. Yang, B. Jia, Z. Yu, Y. Zheng and K. Dai, *Biodegradable Zn–Cu alloys show antibacterial activity against MRSA bone infection by inhibiting pathogen adhesion and biofilm formation*, Acta Biomater. 117 (2020) 400–417.
27. Syamsuir, R. S. Kusumah, A. Premono, A. Lubi, B. Soegijono, S. D. Yudanto et al., *Spinning Effect of Barreling Plating on Physical Properties and Electrochemical Behavior of Copper Layers*, e-Journal Surf. Sci. Nanotechnol. 22 (2024) 120–128.
28. A. C. Larson and R. B. Von Dreele, *General Structure Analysis System (GSAS)*, Vol. 748, University of California, Los Alamos, 2004.
29. R. M. Yusron, R. M. Bisono and M. Pramudia, *Effect Electrolyte Temperature and Electrode Distance to Electroplating Hard-Chrome on Medium-Carbon Steel*, J. Phys. Conf. Ser. 1569 (2020) 042007.
30. X. Qiao, H. Li, W. Zhao and D. Li, *Effects of deposition temperature on electrodeposition of zinc-nickel alloy coatings*, Electrochim. Acta 89 (2013) 771–777.
31. M. A. Lopez-Heredia, P. Weiss and P. Layrolle, *An electrodeposition method of calcium phosphate coatings on titanium alloy*, J. Mater. Sci. Mater. Med. 18 (2007) 381–390.
32. G. Yang, D. Deng, Y. Zhang, Q. Zhu and J. Cai, *Numerical Optimization of Electrodeposition Thickness Uniformity with Respect to the Layout of Anode and Cathode*, Electrocatalysis 12 (2021) 478–488.
33. F. B. Susetyo, B. Soegijono and Yusmaniar, *Effect of a constant magnet position and intensity on a copper layer obtained by DC electrodeposition*, Int. J. Corros. Scale Inhib. 10 (2021) 766–782.
34. Y. Lin, J. Pan, H. F. Zhou, H. J. Gao and Y. Li, *Mechanical properties and optimal grain size distribution profile of gradient grained nickel*, Acta Mater. 153 (2018) 279–289.
35. D. Grujicic and B. Pesic, *Reaction and nucleation mechanisms of copper electrodeposition from ammoniacal solutions on vitreous carbon*, Electrochim. Acta 50 (2005) 4426–4443.
36. Halo Dalshad Omar, *Intensity Correction and Pole Figure Measurement of Copper Metallic by XRD*, J. Basic Appl. Sci. 12 (2016) 320–322.
37. F. Briones, V. Seriacopi, C. Martínez, J. L. Valin, D. Centeno and I. F. Machado, *The effects of pressure and pressure routes on the microstructural evolution and mechanical properties of sintered copper via SPS*, J. Mater. Res. Technol. 25 (2023) 2455–2470.
38. X. Xu, Z. Liu, B. Zhang, H. Chen, J. Zhang, T. Wang et al., *Effect of Mn content on microstructure and properties of 6000 series aluminum alloy*, Appl. Phys. A Mater. Sci. Process. 125 (2019) 1–9.
39. C. O. Ayieko, R. J. Musembi, A. A. Ogacho, B. O. Aduda, B. M. Muthoka and P. K. Jain, *Controlled Texturing of Aluminum Sheet for Solar Energy Applications*, Adv. Mater. Phys. Chem. 05 (2015) 458–466.
40. M. Hubab and M. A. Al-Ghouti, *Recent advances and potential applications for metal-organic framework (MOFs) and MOFs-derived materials: Characterizations and antimicrobial activities*, Biotechnol. Reports 42 (2024) e00837.
41. S. J. Kim, J. Chang and M. Singh, *Peptidoglycan architecture of Gram-positive bacteria by solid-state NMR*, Biochim. Biophys. Acta - Biomembr. 1848 (2015) 350–362.
42. X. Chen, Y. Li, K. Bai, M. Gu, X. Xu, N. Jiang et al., *Class A Penicillin-Binding Protein C Is Responsible for Stress Response by Regulation of Peptidoglycan Assembly in Clavibacter michiganensis*, Microbiol. Spectr. 10 (2022) .
43. S. Xhafa, L. Olivieri, C. Di Nicola, R. Pettinari, C. Pettinari, A. Tombesi et al., *Copper and Zinc Metal–Organic Frameworks with Bipyrazole Linkers Display Strong Antibacterial Activity against Both Gram+ and Gram− Bacterial Strains*, Molecules 28 (2023) 6160.

44. A. Azam, A. S. Ahmed, M. Oves, M. S. Khan and A. Memic, *Size-dependent antimicrobial properties of CuO nanoparticles against Gram-positive and -negative bacterial strains*, Int. J. Nanomedicine 7 (2012) 3527–3535.
45. J. Ramyadevi, K. Jeyasubramanian, A. Marikani, G. Rajakumar and A. A. Rahuman, *Synthesis and antimicrobial activity of copper nanoparticles*, Mater. Lett. 71 (2012) 114–116.
46. M. Ahamed, H. A. Alhadlaq, M. A. M. Khan, P. Karuppiah and N. A. Al-Dhabi, *Synthesis, characterization, and antimicrobial activity of copper oxide nanoparticles*, J. Nanomater. 2014 (2014) .
47. L. Huang, E. M. Fozo, T. Zhang, P. K. Liaw and W. He, *Antimicrobial behavior of Cu-bearing Zr-based bulk metallic glasses*, Mater. Sci. Eng. C 39 (2014) 325–329.
48. M. A. Hajduga, S. Węgrzynkiewicz, J. Waś-Solipiwo, M. Hajduga and M. B. Hajduga, *Innovative solutions from the field of the material science and medicine in the interior of modern ambulances*, Mater. Sci. Forum 844 (2016) 50–54.
49. P. L. Lam, R. S. M. Wong, K. H. Lam, L. K. Hung, M. M. Wong, L. H. Yung et al., *The role of reactive oxygen species in the biological activity of antimicrobial agents: An updated mini review*, Chem. Biol. Interact. 320 (2020) 109023.
50. S. Alfei, G. C. Schito, A. M. Schito and G. Zuccari, *Reactive Oxygen Species (ROS)-Mediated Antibacterial Oxidative Therapies: Available Methods to Generate ROS and a Novel Option Proposal*, Int. J. Mol. Sci. 25 (2024) .
51. A. A. Dayem, M. K. Hossain, S. Bin Lee, K. Kim, S. K. Saha, G. M. Yang et al., *The role of reactive oxygen species (ROS) in the biological activities of metallic nanoparticles*, Int. J. Mol. Sci. 18 (2017) 1–21.
52. A. R. Mir, J. Pichtel and S. Hayat, *Copper: uptake, toxicity and tolerance in plants and management of Cu-contaminated soil*, BioMetals 34 (2021) 737–759.
53. F. N. S. Raja, T. Worthington and R. A. Martin, *The antimicrobial efficacy of copper, cobalt, zinc and silver nanoparticles: alone and in combination*, Biomed. Mater. 18 (2023) 045003.
54. S. Y. Tsai, Y. M. Liu, Z. W. Lin and C. P. Lin, *Antimicrobial activity effects of electrolytically generated hypochlorous acid-treated pathogenic microorganisms by isothermal kinetic simulation*, J. Therm. Anal. Calorim. 148 (2023) 1613–1627.
55. D. Marković, C. Deeks, T. Nunney, Ž. Radovanović, M. Radoičić, Z. Šaponjić et al., *Antibacterial activity of Cu-based nanoparticles synthesized on the cotton fabrics modified with polycarboxylic acids*, Carbohydr. Polym. 200 (2018) 173–182.
56. Ž. Z. Tasić, M. B. Petrović Mihajlović, M. B. Radovanović and M. M. Antonijević, *Electrochemical investigations of copper corrosion inhibition by azithromycin in 0.9% NaCl*, J. Mol. Liq. 265 (2018) 687–692.
57. C. Zheng, J. Cao, Y. Zhang and H. Zhao, *Insight into the Oxidation Mechanism of a Cu-Based Oxygen Carrier (Cu → Cu2O → CuO) in Chemical Looping Combustion*, Energy and Fuels 34 (2020) 8718–8725.
58. B. Narayanan, S. A. Deshmukh, S. K. R. S. Sankaranarayanan and S. Ramanathan, *Strong correlations between structural order and passive state at water-copper oxide interfaces*, Electrochim. Acta 179 (2015) 386–393.
59. S. Ghosh, *Electroless copper deposition: A critical review*, Thin Solid Films 669 (2019) 641–658.